# Structural evolution across the insulator-metal transition in oxygen-deficient BaTiO_{3−δ} studied using neutron total scattering and Rietveld analysis

I.-K. Jeong, Seunghun Lee, Se-Young Jeong, C. J. Won, N. Hur, and A. Llobet

Phys. Rev. B **84**, 064125 — Published 29 August 2011

DOI: 10.1103/PhysRevB.84.064125

# Structural evolution across insulator-metal transition in oxygen deficient $BaTiO_{3-\delta}$ studied using neutron total scattering and Rietveld analysis

I.-K. Jeong[1],* Seunghun Lee[2], Se-Young Jeong[2], C. J. Won[3], N. Hur[3], and A. Llobet[4]
[1] *Department of Physics Education & Research Center for Dielectrics and Advanced Matter Physics, Pusan National University, Busan, 609-735, Korea.* [2] *Department of Cogno-Mechatronics Engineering, Pusan National University, Miryang, 627-706, Korea.* [3] *Department of Physics, Inha University, Incheon, 402-751, Korea.* [4] *Los Alamos National Laboratory, Lujan Neutron Science Center, MS H805, Los Alamos, NM 87545, USA.*

Oxygen deficient $BaTiO_{3-\delta}$ exhibits insulator-metal transition with increasing $\delta$. We performed neutron total scattering measurements to study structural evolution across insulator-metal transition in $BaTiO_{3-\delta}$. Despite its significant impact on resistivity, slight oxygen reduction ($\delta$=0.09) caused little disturbance on local doublet splitting of Ti-O bond. This finding implies that local polarization is well preserved under marginal electric conduction. In the highly oxygen deficient metallic state ($\delta$=0.25), however, the doublet splitting of Ti-O bond became smeared. The smearing of local Ti-O doublet is complemented with long-range structural analysis and demonstrates that the metallic conduction in the highly oxygen reduced $BaTiO_{3-\delta}$ is due to the appearance of non-ferroelectric cubic lattice.

PACS numbers: 77.84.-s, 61.43.Gt, 61.50.Ks, 61.05.fg

## I. INTRODUCTION

Oxygen vacancy is one of the common defects in perovskite ferroelectrics[1] and is known to cause significant impact on electronic transport properties[2,3]. From the structural viewpoint, oxygen vacancies also have important effect on electric polarization by distorting oxygen cage of a ferroelectric active ion. Thus, it can be speculated that electrical conduction and ferroelectric ordering will have close relation in perovskite ferroelectrics via oxygen deficiency. In fact, a polarization dependent diode and photovoltaic effect were reported in leaky ferroelectrics such as $BiFeO_3$[4] and $BaTiO_{3-\delta}$[5].

According to systematic studies on oxygen deficient $BaTiO_{3-\delta}$ single crystals[6], insulator-metal transition occurs with increasing oxygen vacancies. Across the insulator-metal transition, however, structural distortion caused by the oxygen deficiency is not well understood. As itinerant electrons screen Coulombic fields which is responsible for ferroelectric distortions[7], one may expect that structural distortion disappears in the metallic state, and thus metallic conduction and ferroelectric ordering are not compatible with each other. To investigate crystal symmetry of $BaTiO_{3-\delta}$ in the metallic phase[8], Kolodiazhnyi *et al.* performed x-ray diffraction studies as a function of temperature. In contrary to the conventional expectation, the authors reported a series of low symmetry structural transitions in the metallic state and claimed that ferroelectricity persists through the insulator-metal transition of $BaTiO_{3-\delta}$.

In this paper, we studied local and long-range structure of $BaTiO_{3-\delta}$ in the insulating and metallic states using neutron total scattering analysis[9] as well as Rietveld refinement. In $BaTiO_3$, an off-centering of Ti ion with respect to the oxygen octahedron is the source of the local polarization. If the metallic state of $BaTiO_{3-\delta}$ maintains ferroelectricity, then the off-center behavior of Ti ion and an ordering among them should be preserved as well. Thus, local and long-range structural approaches complement with each other in understanding structural evolution in oxygen deficient $BaTiO_{3-\delta}$.

## II. EXPERIMENTS AND ANALYSIS

Powder sample of $BaTiO_3$ was synthesized using a conventional solid state reaction. Oxygen deficient specimens were obtained by post-annealing $BaTiO_3$ powder with Zr foils in a sealed silica tube at 700° (#1), 900° (#2) and 1100°C (#3), respectively. From energy dispersive x-ray (EDX) spectroscopy, oxygen reduction ($\delta$) of sample #2 and #3 were estimated as 0.09 and 0.25, respectively. For the sample #1, the composition was not reliably differentiated from stoichiometric $BaTiO_3$ using EDX measurement although a comparison of resistivity with that of single crystal $BaTiO_{2.98}$ suggests that the oxygen reduction will be larger than 0.03. To indicate that the sample #1 has almost stoichiometric composition, we will designate it as $BaTiO_3$ (#1). Figure 1 shows the electrical resistivity of $BaTiO_{3-\delta}$ as a function of temperature. With increasing reduction of oxygen content, resistivity decreases drastically and temperature dependent behavior changes from insulating to metallic, consistent with previous studies[6].

Neutron powder diffraction experiments were performed at room temperature on the NPDF instrument at the Los Alamos Neutron Science Center. For the total scattering analysis, structure function S(Q) which contains both Bragg & diffuse scattering was determined up to the magnitude of wavevector Q=30 $Å^{-1}$ from neutron powder diffraction measurements after corrections for experimental effects and normalization by incident neutron flux using program PDFgetN[10]. Real-space pair distribution function (PDF), G(r) is obtained by a sine Fourier transform of S(Q) i. e. $G(r) = 4\pi r[\rho(r) - \rho_0] = \frac{2}{\pi}\int_0^{Q_{max}} Q[S(Q) - 1]\sin Qr\, dQ$. Here, $r$ is the atomic pair distance, $\rho(r)$, and $\rho_0$ are atomic number density and average number density, respectively.

## III. RESULTS AND DISCUSSION

Figure 2(a) shows a total scattering structure function, Q[S(Q)-1] of $BaTiO_3$ (#1). The corresponding real-space PDF spectrum is shown in Fig. 2(b). Here, the first PDF peak appears as a negative peak as Ti ion has a negative neutron scattering length. Also note that the six-fold degeneracy of Ti-O bond is broken due to an off-centering of Ti ion in oxygen octahedron and tetragonal distortion. From the shape of the well-resolved doublet, we can reasonably speculate that Ti ion is off-centered toward [111] direction. For comparison, the inset shows model Ti-O bond length distribution assuming [111] Ti off-centering. As $BaTiO_3$ has a long-range tetragonal structure at room temperature, it is expected that Ti ion displaces along [001] direction. However, Ti off-centering along [001] direction will result in a splitting of Ti-O bond into one short-bond, four medium-length bond, and one long-bond. Thus, the [111] off-centering of Ti ion found in Fig. 2(b) suggests a discrepancy between local symmetry of Ti ion and long-range tetragonal crystal symmetry at room temperature. In fact, x-ray absorption fine structure measurements[11] as well as the first principle studies[13] showed that local structure of $BaTiO_3$ remains identical at all temperatures regardless

of its long-range average crystal symmetry. Thus, even above the Curie temperature when the crystal has cubic symmetry, Ti ions are off-centered along eight equivalent <111> directions. With decreasing temperature, these local off-centering develop order-disorder type antiferroelectric coupling[12–15] in one, two, and three dimensions. As a result, the crystal undergoes long-range phase transition to orthorhombic, tetragonal, and cubic structures, respectively.

Figure 3(a) shows the Ti-O bond length distributions for three samples of $BaTiO_{3-\delta}$. Between $BaTiO_3$(#1) and $BaTiO_{2.91}$, the Ti-O doublet is little changed although the resistivity is significantly reduced with slight oxygen reduction (Fig. 1). This result implies that local polarization is well maintained under marginal electrical conduction. In contrast, the gap between the two Ti-O peaks is almost completely filled in the highly oxygen deficient $BaTiO_{2.75}$. Figure 3(b) shows a simple model for the smeared Ti-O doublet. The model Ti-O bond length distribution is obtained by assuming two contributions: doublet Ti-O bonds due to Ti [111] displacement and single Ti-O bond with Ti ion at the center of octahedron. The reasonable agreement between experimental and model Ti-O bond distribution suggests important implication on the origin of the smearing that the sample may have two distinct phases, one with distorted Ti-O bond and the other with undistorted Ti-O bond as the oxygen deficiency increases.

Beyond the nearest neighbor Ti-O bond distance, PDF spectra of the insulating $BaTiO_3$(#1) and the metallic $BaTiO_{2.75}$ match quite well with each other as shown in Fig. 4(a). At higher pair distances above $r \sim$35 Å, however, the two spectra become discernible. In Fig. 4(b), note that PDF peaks of the metallic state are sharper than those in the insulating state. As PDF peak width represents static and thermal disorder[16], we expect that highly oxygen deficient $BaTiO_{2.75}$ will have broader PDF peaks due to structural disorder. However, what we found is that PDF peaks are sharper in disordered $BaTiO_{2.75}$. One plausible explanation is assuming that the average lattice distortion decreases with increasing oxygen reduction.

Finally, we examined long-range crystal structure of $BaTiO_{3-\delta}$. Figure 5(a) shows a part of neutron powder diffraction pattern near <200> peak. For the insulating $BaTiO_3$(#1) and $BaTiO_{2.91}$, cubic <200> peak splits into two Bragg peaks due to the tetragonal distortion. In contrast, the corresponding Bragg peak in the metallic $BaTiO_{2.75}$ shows a three-peak structure which is an indicative of a new crystallographic structure.

To obtain detailed long-range structural information, Rietveld refinement was performed for the diffraction patterns of $BaTiO_{3-\delta}$ using GSAS[17]. For $BaTiO_3$(#1) and $BaTiO_{2.91}$, single tetragonal structure (P4mm) was used for the refinement (not shown). In the case of $BaTiO_{2.75}$, however, a mixed phase of tetragonal (P4mm) and cubic (Pm3m) structures was used as shown in Fig. 5(b) and an excellent match was obtained. The inset shows the fitting for the Bragg peak near <200> reflection.

Table 1 summarizes structural information such as lattice parameters and atomic positions obtained from Rietveld refinement. As we discussed earlier, Ti ions are locally off-centered along equivalent <111> directions at all crystal structures. In the average structure refinement, however, we assumed that Ti ion displaces along [001] direction in the tetragonal structure and stays at the center of the octahedron in the cubic structure[18]. We also tried to refine the occupancy of oxygen content. However, the oxygen occupancy remains close to one for all samples including $BaTiO_{2.75}$. We expect that this result is due to a coupling of disorder on oxygen positions and oxygen occupancy. As both atomic positions and content influence Bragg peak intensities, the oxygen content will not be reliably refined without having good knowledge of oxygen positions. In disordered material like $BaTiO_{2.75}$ we only have information on average atomic positions. Between $BaTiO_3$(#1) and $BaTiO_{2.91}$, tetragonality value of c/a ratio decreases from 1.010(1) to 1.008(1). However, no further decrease of c/a ratio was observed in $BaTiO_{2.75}$. It is also worth to note that the displacement of Ti ion gradually increases with increasing oxygen deficiency. This is an indication of close interplay between oxygen vacancies and Ti displacement. In addition, the two-phase modeling for the highly oxygen deficient $BaTiO_{2.75}$ showed that the amount of cubic phase is about 60%. This result complements local structural finding of the smeared Ti-O doublet (Fig. 3(b)) and suggests an appearance of average cubic lattice out of the tetragonal lattice in $BaTiO_{2.75}$.

## IV. CONCLUSION

Neutron total scattering analysis of $BaTiO_{3-\delta}$ showed that local distortion of Ti-O bond is stable in insulating state with slight oxygen reduction ($\delta$=0.09). In the highly oxygen deficient metallic $BaTiO_{2.75}$, however, distorted and undistorted Ti-O bonds were found to coexist. This local structural analysis is complemented with the long-range structural refinement which suggests a mixed phase of tetragonal and cubic structure in $BaTiO_{2.75}$. These structural results provide insight in understanding insulator-metal transition in $BaTiO_{3-\delta}$ with increasing oxygen deficiency. As shown in Nb substituted $BaTiO_3$ and $SrTiO_3$ the presence or disappearance of Ti-O distortion causes crucial influence in conduction behavior. For example, Ti/Nb-O bond is distorted in semiconducting $BaTi_{0.875}Nb_{0.125}O_3$. In contrast, $SrTi_{0.875}Nb_{0.125}O_3$[19] exhibits metallic behavior with undistorted Ti/Nb-O bond. Similarly, the two-phase mixture of $BaTiO_{2.75}$ suggests that the metallic conduction is due to the part of cubic phase with undistorted Ti-O bond and remaining ferroelectric tetragonal phase is insulating. Therefore, we conclude that the ferroelectric ordering and

metallic conduction are not coexisting phases but are two distinct phases of the material.

## ACKNOWLEDGMENTS

This work was supported by the National Research Foundation of Korea grant funded by the Korean Government (MEST) No. 2009-0073785 and No. 2010-00001198. Neutron diffraction measurements have benefited from the use of NPDF and HIPD at the Lujan Center at Los Alamos Neutron Science Center, funded by DOE Office of Basic Energy Sciences. Los Alamos National Laboratory is operated by Los Alamos National Security LLC under DOE Contract DE-AC52-06NA25396. The upgrade of NPDF has been funded by NSF through grant DMR 00-76488.

---

* To whom correspondence should be addressed. E-mail:Jeong@pusan.ac.kr

[1] D. M. Smyth, Annu. Rev. Mater. Sci. **15**, 329 (1985).
[2] C. N. Berglund and W. S. Baer, Physical Review **157**, 358 (1967).
[3] T. Mihara, H. Watanabe, and C. A. P. de Araujo, Jpn. J. Appl. Phys. Part 1 **33**, 5281 (1994).
[4] T. Choi, S. Lee, Y. J. Choi, V. Kiryukhin, and S.-W. Cheong, Science **324**, 63 (2009).
[5] C. J. Won, Y. A. Park, K. D. Lee, H. Y. Ryu, and N. Hur, Journal of Applid Physics **109**, 084108 (2011).
[6] T. Kolodiazhnyi, Phys. Rev. B **78**, 045107 (2008).
[7] I. A. Sergienko, V. Keppens, M. McGuire, R. Jin, J. He, S. H. Curnoe, B. C. Sales, P. Blaha, D. J. Singh, K. Schwarz, and D. Mandrus, Phys. Rev. Lett. **92**, 065501 (2004).
[8] T. Kolodiazhnyi, M. Tachibana, H. Kawaji, J. Hwang, and E. Takayama-Muromachi, Phys. Rev. Lett. **104**, 147602 (2010).
[9] T. Egami and S. J. L. Billinge, *Underneath the Bragg Peaks: Structural Analysis of Complex Materials* (Pergamon Press, Oxfore, UK, 2003).
[10] P. F. Peterson, M. Gutmann, T. Proffen, and S. J. L. Billinge, J. Appl. Cryst. **33**, 1192 (2000).
[11] B. Ravel, E. A. Stern, R. I. Vedrinskii, and V. Kraisman, Ferroelectrics **206** (1998).
[12] E. A. Stern, Phys. Rev. Lett. **93**, 037601 (2004).
[13] Q. Zhang, T. Cagin, and W. A. G. III, PNAS **103**, 14695 (2006).
[14] C. Laulhe, F. Hippert, R. Bellissent, A. Simon, and G. J. Cuello, Phys. Rev. B **79**, 064104 (2009).
[15] I.-K. Jeong, C. Y. Park, J. S. Ahn, S. Park, and D. J. Kim, Phys. Rev. B **81**, 214119 (2010).
[16] I.-K. Jeong, T. W. Darling, J. K. Lee, T. Proffen, R. H. Heffner, J. S. Park, K. S. Hong, W. Dmowski, and T. Egami, Phys. Rev. Lett. **94**, 147602 (2005).
[17] A. C. Larson and R. B. Von Dreele, *General Structure Analysis System*, unpublished Report LAUR 86-748 (Los Alamos National Laboratory, 1986).
[18] F. Jona and G. Shirane, *Ferroelectric Crystals* (Dover Pub. Inc., New York, 1993).
[19] K. Page, T. Kolodiazhnyi, T. Proffen, A. K. Cheetham, and R. Seshadri, Phys. Rev. Lett. **101**, 205502 (2008).

FIG. 1. (color online) Temperature dependence of resistivity for $BaTiO_{3-\delta}$ samples post-annealed in a reduced condition at 700°C, 900°C, and 1100°C, respectively. The resistivity changes from insulating (#1, #2) to metallic (#3) behavior.

FIG. 2. (color online) (a) Neutron total scattering structure function, Q[S(Q)-1], of $BaTiO_3$ (#1) at 300 K. (b) Corresponding Pair Distribution Function. Note that the first peak appears as a negative peak due to a negative neutron scattering length of Ti ion. The inset shows the model Ti-O bond length distribution assuming Ti ion displaced toward [111] direction within the oxygen octahedron.

FIG. 3. (color online) (a) Ti-O bond length distribution of three $BaTiO_{3-\delta}$ samples. For clarity, distribution functions are shifted vertically from each other. Note that Ti-O doublet is well resolved in the sample $BaTiO_3$(#1) & $BaTiO_{2.91}$ (insulating) but the splitting became smeared in the metallic $BaTiO_{2.75}$. (b) Comparison of Ti-O bond length distribution for $BaTiO_{2.75}$ with model calculation. Model Ti-O bond length distribution is composed of two contributions: doublet Ti-O bonds due to Ti [111] displacement and single Ti-O bond with Ti ion at the center of octahedron.

FIG. 4. (color online) Comparison of PDF spectra between $BaTiO_3$(#1) and $BaTiO_{2.75}$ in different $r$-ranges. (a) In the $r$-range, 3.5 Å<r<20 Å both samples have basically identical atomic pair distributions. (b) In higher $r$-range (34 Å<r<50 Å), the two PDF spectra become discernible; PDF peaks in the metallic $BaTiO_{2.75}$ are sharper than those in the insulating state.

FIG. 5. (color online) (a) Powder diffraction patterns of $BaTiO_{3-\delta}$ samples. (b) Rietveld fitting of the $BaTiO_{2.75}$. The fit (line) is obtained using mixed tetragonal (T) and cubic (C) phases. The inset shows a part of the fitting around <200> Bragg peak. Tick marks for cubic and tetragonal phases are shown with difference curve. Weighted R-factor, $R_{wp}$=2.75%. In the cubic phase, all atoms sit at high symmetry positions.

TABLE I. Atomic parameters of $BaTiO_{3-\delta}$ obtained from Rietveld refinements. In tetragonal phase, atoms are located at the following sites: Ba at (0,0,0). Ti at (0.5, 0.5, 0.5+$\delta z_{Ti}$), O1 at (0.5, 0.5, $\delta z_{O1}$), and O2 at (0.5, 0.0, 0.5+$\delta z_{O2}$)[18]. For $BaTiO_{2.75}$, tetragonal-cubic mixed phase fitting was performed. The refined ratio of tetragonal and cubic phases is about 4:6.

| | | $BaTiO_3$ (#1) | $BaTiO_{2.91}$ | $BaTiO_{2.75}$ | |
|---|---|---|---|---|---|
| Space Group | | P4mm | P4mm | P4mm (41 %) | Pm3m (59%) |
| Lattice | a | 3.99307(5) | 3.99547(7) | 3.99545(5) | 4.00700(4) |
| parameters (Å) | c | 4.03238(6) | 4.02744(9) | 4.02864(8) | - |
| Shifts of atoms | $\delta z_{Ti}$ | 0.009(1) | 0.013(2) | 0.021(1) | 0.0 |
| | $\delta z_{O1}$ | -0.028(1) | -0.025(1) | -0.024(1) | 0.0 |
| | $\delta z_{O2}$ | -0.019(1) | -0.013(2) | -0.008(2) | 0.0 |
| Rwp (%) | | 3.27 | 2.98 | 2.75 | |
| Rp (%) | | 2.08 | 1.91 | 1.81 | |

Caption: Figure 1
Caption: Figure 2
Caption: Figure 3
Caption: Figure 4
Caption: Figure 5
Caption: Table 1

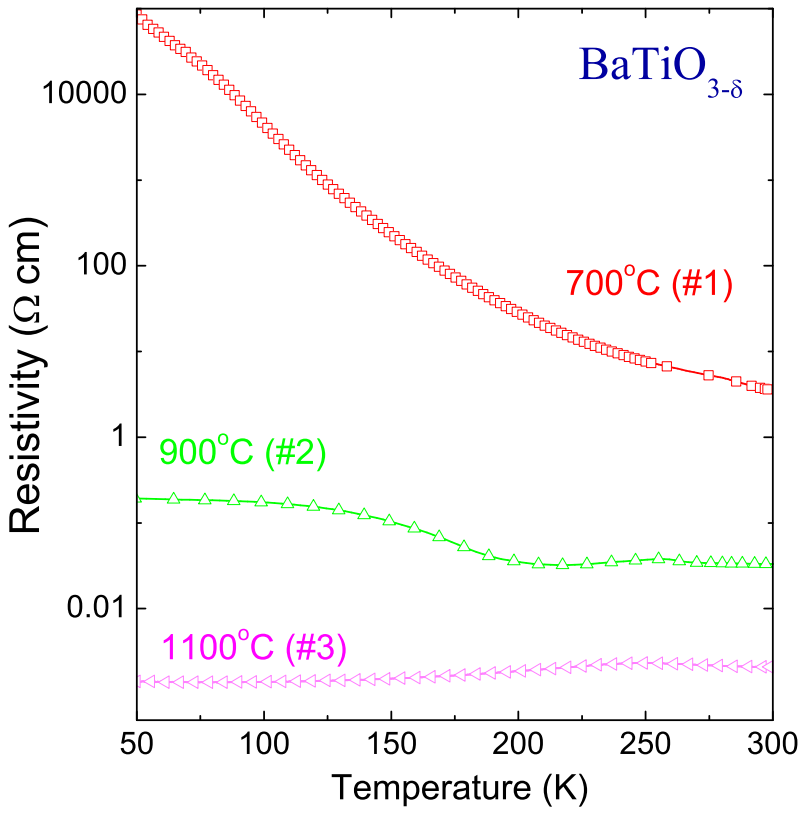


Figure 1 LE13656 15Jul2011

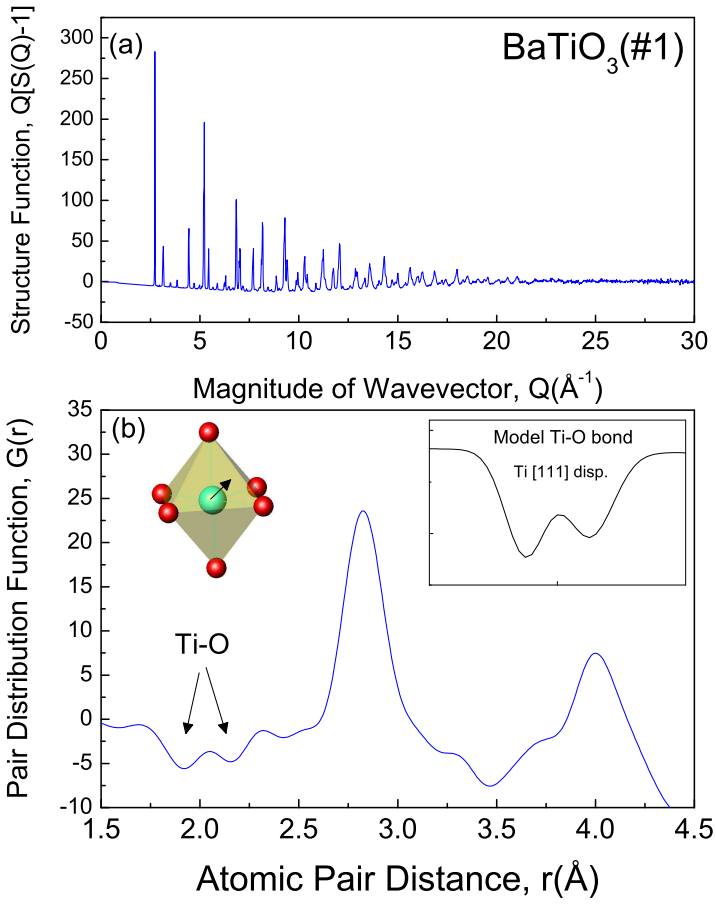


Figure 2 LE13656 15Jul2011

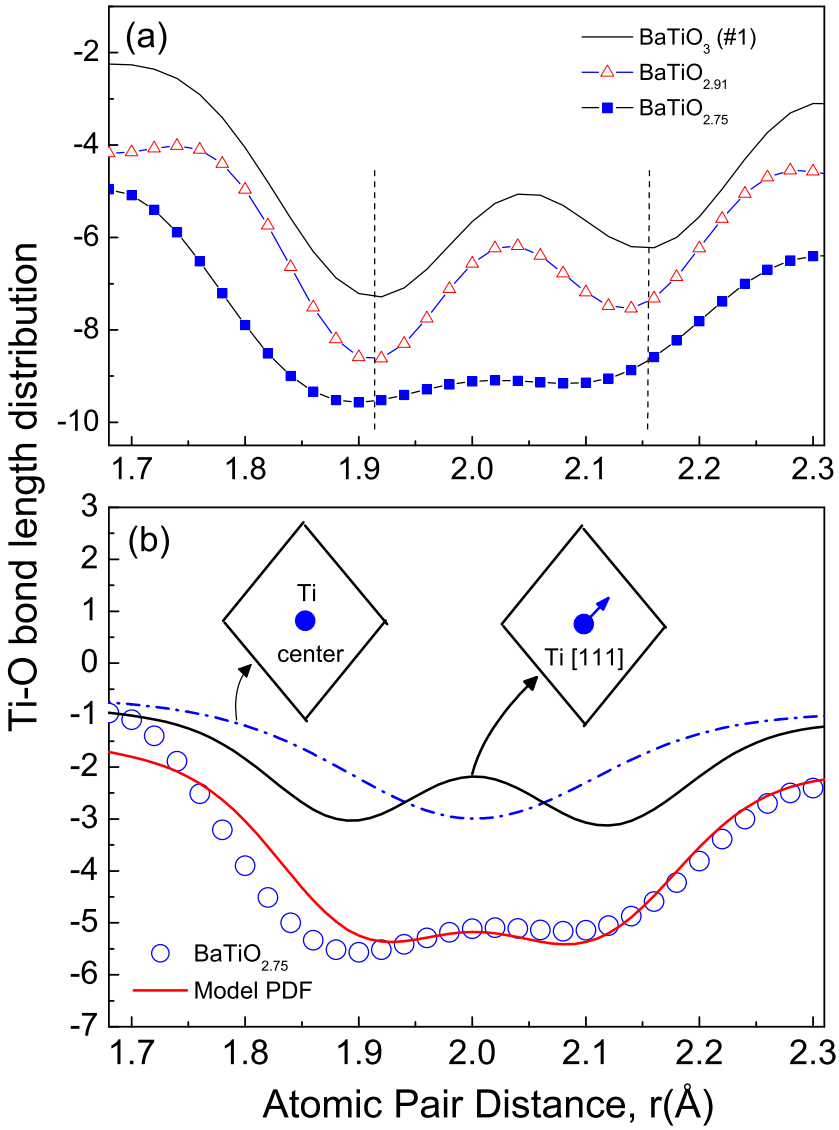


Figure 3 LE13656 15Jul2011

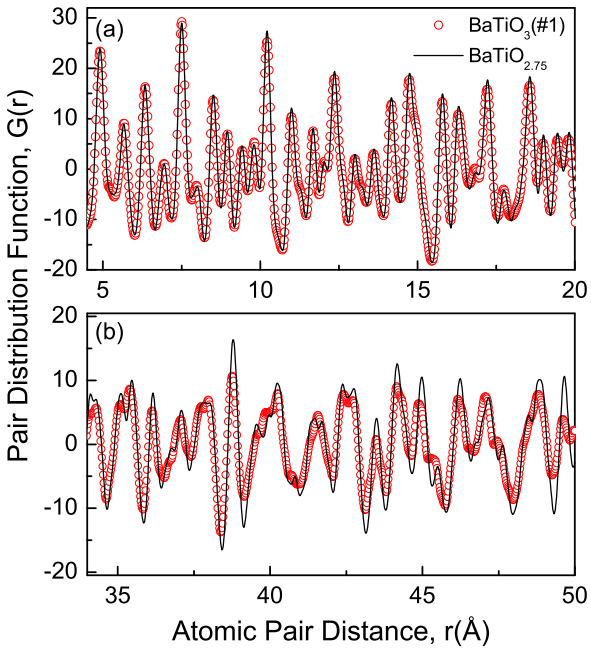


Figure 4 LE13656 15Jul2011

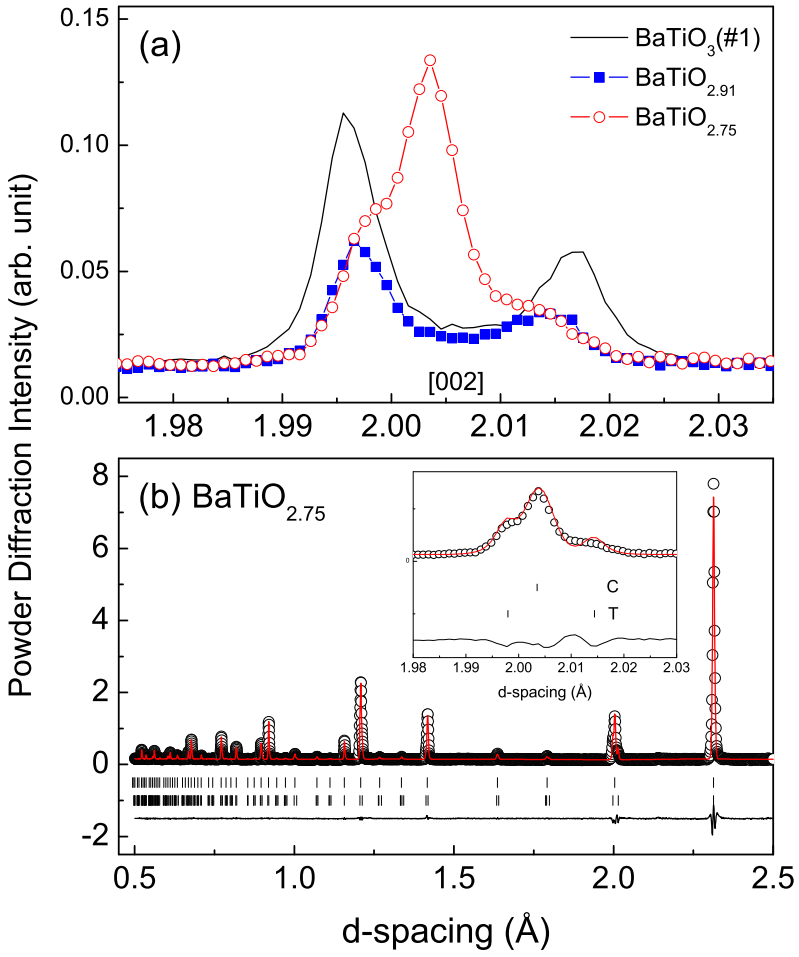


Figure 5 LE13656 15Jul2011